Cerebrovascular damages induce lymphatic invasion into brain parenchyma to guide vascular regeneration

Jingying Chen[1], Jianbo He[1], Qifen Yang[1], Yaoguang Zhang[1], Tianyu Zhao[2], Deqin Yang[2,*] and Lingfei Luo[1,*]

[1]Key Laboratory of Freshwater Fish Reproduction and Development, Ministry of Education, Laboratory of Molecular Developmental Biology, School of Life Sciences, Southwest University, Beibei, 400715 Chongqing, China

[2]Department of Endodontics and Operative Dentistry, Chongqing Key Laboratory for Oral Diseases and Biomedical Sciences, The Affiliated Hospital of Stomatology, Chongqing Medical University, 401147 Chongqing, China.

Correspondence should be addressed to L.L. (email: lluo@swu.edu.cn) and D.Y. (email: yangdeqin@hospital.cqmu.edu.cn)

Damage to regional brain vasculature and neuronal tissues occurs during acute cerebrovascular diseases, such as ischemic stroke. Promoting vascular regeneration is the most promising therapeutic approach. To understand cellular and molecular mechanisms underlying brain vascular regeneration, we developed two zebrafish cerebrovascular injury models using genetic ablation and photochemical thrombosis. Although brain parenchyma is physiologically devoid of lymphatic vasculature, we found that cerebrovascular injuries induce rapid ingrowth of meningeal lymphatics into the injured parenchyma. The ingrown lymphatics on one hand become lumenized

to drain interstitial fluid to resolve brain oedema, on the other hand act as "growing tracks" for nascent blood vessels and produce Vegfa to promote the neoangiogenesis. The ingrown lymphatic vessels undergo apoptosis and clearance after cerebrovascular regeneration. This study reveals a pathological function of meningeal lymphatics, through previously unexpected ingrowth into brain parenchyma and a newly identified lymphatic function as vascular "growing tracks".

Ischemic stroke develops when a blood vessel supplying blood to a brain area is blocked. It causes injury to the regional vascular and neuronal tissues and becomes a major cause of death and adult disability[1-2]. Promotion of cerebrovascular regeneration, involving the growth of nascent blood vessels (neoangiogenesis) into the post-ischemic infarction area, is a prerequisite to re-nourish the injured brain parenchyma thus becoming the most promising therapeutic approach[3-4]. Angiogenic signals including factors and proteases such as VEGF, PDGF and matrix metalloproteinases have been reported to originate from injured neurons, reactive astrocytes and blood vessels[5-7]. However, studies have yet to be made to understand cellular and molecular mechanisms underlying how the injured brain parenchyma becomes revascularized.

Lymphatic vessels play essential roles in fluid homeostasis, fat absorption, and several pathological processes including lymphedema and tumor metastasis. Despite recent discovery of meningeal lymphatics including meningeal lymphatic vessels in

mouse and mural lymphatic endothelial cells (muLECs) in zebrafish[8-12], the brain parenchyma is devoid of lymphatic vessels under physiological conditions. Whether lymphatic vessels are able to invade brain parenchyma and whether meningeal lymphatics play roles under pathological circumstances are unknown.

Results

Establishment of a brain vascular injury-regeneration model in zebrafish

The zebrafish model system has substantially contributed to the understanding of angiogenesis and lymphangiogenesis during embryonic development[13-15] as well as organ regeneration[16-19]. To study brain vascular regeneration, we established a zebrafish cerebrovascular injury model using the NTR-Mtz system[18,19]. The *Tg(kdrl:DenNTR)*^{cq10} transgenic line was generated, with Dendra2 (Den) fused to NTR and driven by the vascular-specific promoter *kdrl*. Controlled by the *Tg(kdrl:DenNTR)* larvae treated with DMSO (Fig. 1a) and *Tg(kdrl:GFP)* larvae treated with Mtz (Supplementary Fig. 1a), incubation of the *Tg(kdrl:DenNTR)* larvae at 3 days post fertilization (3 dpf) with Mtz led to ablation of a majority of regional cerebrovascular endothelial cells (ECs) at 0 days post treatment (0 dpt, equivalent to 4 dpf), but left some larger vessels intact (Fig. 1b, arrowheads). Because blood vessel ECs (BECs) in the brain are more sensitive to Mtz than those in the trunk, specific injury to brain blood vessels was achieved using a low concentration (1 mM) of Mtz, without affecting trunk vasculature or generating body phenotypes (Supplementary Fig. 1c).

Widespread apoptotic signals were detected in the brain after Mtz treatment, including endothelial and neuronal tissues (Supplementary Fig. 1d,e). Local haemorrhages appeared in the brain (Supplementary Fig. 1f,g), mimicking the symptoms of massive ischemic stroke. Macrophage infiltration and engulfment of dead cells were observed (Supplementary Fig. 1h,i). All these data demonstrate that Mtz treatment damages the local cerebrovascular network and generates an injured area in the brain. The emergence of neoangiogenesis from the peri-injured into the injured area was observed at 1 dpt (Fig. 1b, arrows). This regeneration process proceeded at 2 dpt, became evident at 5 dpt, and completed at 7-8 dpt (Fig. 1b and Supplementary Fig. 1b).

Brain vascular injury induces a Vegfc-dependent ingrowth of meningeal lymphatics into the injured parenchyma

Using the *lyve1b* or *prox1a* promoter-driven transgenes to label lymphatic vessels[20,21], we found rapid and active ingrowth of lymphatics into the injured area on the first day after cerebrovascular injury, but apparently slowed by the second day (Fig. 1, c–e, and Supplementary Fig. 2). Frontier sections of the brain showed that lymphatics were only present in the meninges at the brain surface under physiological conditions (Fig. 1f, #1), but became abundant in the brain parenchyma at 1 dpt after injury (Fig. 1f, #1'). Meningeal lymphatics/muLECs turn out to be the only known lymphatic ECs (LECs) inside zebrafish skull[10-12]. So, we investigate whether lymphatics in the

parenchyma are actually the ingrown meningeal lymphatics after injury. Time-lapse live imaging illustrated a rapid growth of meningeal lymphatics into the injured parenchyma at 0-1 dpt (Fig. 2a and Supplementary Video 1). The initiation of lymphatic ingrowth and branching at the early phase post-injury was exhibited by 3D-reconstructions (Fig. 2b and Supplementary Video 2). To further substantiate that the ingrown vessels are of the lymphatic origin, Cre/loxP-based lineage tracing was performed using the *Tg(lyve1b:CreER^{T2}; β-actin:loxP-RFP-loxP-GFP; lyve1b:DsRed; kdrl:DenNTR)* line (Fig. 2c). Negatively controlled by Mtz plus ethanol (Fig. 2d) and positively controlled by DMSO plus 4-hydroxytamoxifen (4-OHT; Fig. 2e), most ingrown lymphatics were double positive for both GFP and DsRed if Mtz plus 4-OHT were applied (Fig. 2f,g). All the results above demonstrate that meningeal lymphatics respond to cerebrovascular injury and rapidly grow into the injured brain parenchyma.

Active lymphangiogenesis requires lymphangiogenic factors. Using *kdrl:DenNTR* and *nkx2.2:GFP* transgenes, fluorescent *in situ* hybridizations (FISH) showed activation of the classical pro-lymphangiogenic marker *vegfc* in the remaining BECs and a portion of *nkx2.2*-positive neurons, inside and at the border of the injured area at 1 dpt (Fig. 3a,b and Supplementary Fig. 3a,b). Activation of *vegfc* dramatically reduced at 3 dpt and reached the bottom level at 4-5 dpt (Fig. 3c). Vegfr3, the Vegfc receptor, was exclusively expressed in the ingrown LECs and kept absent in the BECs (Fig. 3d–f and Supplementary Fig. 3c–e). These expression patterns suggest that residual BECs and neurons secrete the pro-lymphangiogenic factor Vegfc to act on LECs, thus promoting the ingrowth of meningeal lymphatics. To make sure the

functional significance of Vegfc for the ingrowth of meningeal lymphatics, we applied the *ccbe1* mutant. Ccbe1 is required for the processing and maturation of Vegfc, thereby its mutation causes defective lymphangiogenesis[22-24]. Although the *ccbe1* mutant exhibited defects in lymphatic development and slight cerebral oedema as indicated by the inter-optic distance, its brain vasculature remained normal (Supplementary Fig. 4). However, ingrowth of meningeal lymphatics (*fli1*+*kdrl*-) and cerebrovascular regeneration (*kdrl*+) failed to occur in the mutant after injury (Fig. 3g–j). The mutant died from severe cerebral oedema at 3 dpt (Fig. 3k–m). These results on one hand ensure the requirement of Vegfc for the meningeal lymphatic ingrowth, on the other hand imply roles of the ingrown lymphatic vessels in oedema resolvation and cerebrovascular regeneration. The rest of the study will focus on the functions of the ingrown meningeal lymphatics.

The ingrown meningeal lymphatics become lumenized to drain brain interstitial fluid

Severe brain vascular injury usually leads to cerebral oedema[5]. The lethal oedema in the *ccbe1* mutant (Fig. 3k–m) provides evidences that the ingrown meningeal lymphatics drain interstitial fluid from the injured brain to resolve oedema. Because zebraifsh meningeal lymphatics are nonlumenized under physiological conditions[10-12], we investigate whether the ingrown lymphatics become lumenized and gain the interstitial fluid drainage function. Controlled by the dorsal aorta (DA) injection of Rhodamine-Dextran that labelled the lumen of blood vessels, intracerebroventricular

(ICV) injection labelled brain interstitial fluid. Drainage of Rhodamine was observed in the lumen of *fli1+kdrl-* lymphatic vessels immediately after the ICV injection (Fig. 4a–c), demonstrating that lumenized lymphatic vessels have been formed and interstitial fluid drainage function has been obtained at 3 dpt. Then, we performed ICV injection of Alexa647-IgG (150 kDa) at 1 dpt and 2 dpt to learn approximately when the lumenization occurred. Similar to the control[12] (Fig. 4d), the ingrown meningeal lymphatics remained nonlumenized and the LECs kept endocytose the Alexa647-IgG macromolecules at 1 dpt (Fig. 4f). The endocytosed Alexa647-IgG maintained and accumulated in the LECs thirty minutes after injection (Fig. 4e,g). Lumen of the ingrown meningeal lymphatics appeared at 2 dpt (Fig. 4h, arrows). Alexa647-IgG filled in the lumen immediately after the ICV injection, then became drained out thirty minutes later (Fig. 4i). The focused ion beam scanning electron microscopy (FIB-SEM) analyses later will provide further evidences that the ingrown meningeal lymphatics were lumenized at 2 dpt (Fig. 5h). All these data demonstrate that the ingrown meningeal lymphatics undergo a lumenization process between 1 dpt and 2 dpt, thus becoming functional to drain interstitial fluid to resolve cerebral oedema.

The ingrown lymphatics act as "growing tracks" for nascent blood vessels and produce Vegfa to promote the neoangiogenesis

Based on phenotypes of the *ccbe1* mutant (Fig. 3h), we next explore roles of the ingrown meningeal lymphatics in brain vascular regeneration. Nascent blood vessels were observed growing along the preformed, ingrown lymphatics (Fig. 5a and Supplementary Video 3). When the ingrown lymphatics were specifically ablated by the focused irradiation of high-energy multi-photon laser, the nascent blood vessel growing alongside exhibited growth arrest and regression. In contrast, the ablation of parenchymal tissues neighbouring the lymphatics did not affect the growth of nascent blood vessel (Fig. 5b,c and Supplementary Video 4). These data suggest the ingrown lymphatics as "growing tracks" for nascent blood vessels, most likely through direct physical adhesion. This physical adhesion was supported by the enrichment of surface adhesion molecules Claudin5b and Cdh5 at the interface between the ingrown lymphatic and adjacent blood vessels at 2 dpt (Fig. 5d,e and Supplementary Fig. 5), proposing the paracellular interaction between BECs and LECs. Correlative light and electron microscopy (CLEM) and 3D-reconstructions of FIB-SEM substantiated the ingrown meningeal lymphatics and nascent blood vessels as two adhering vessel structures with lumens (Fig. 5f–h and Supplementary Video 5). All these results demonstrate that the ingrown meningeal lymphatics act as "growing tracks" to support and guide the growth of nascent blood vessels.

Active neoangiogenesis requires pro-angiogenic factors. Zebrafish meningeal LECs can produce Vegfa to regulate meningeal angiogenesis during development[10], implying their further functions in cerebrovascular regeneration as pro-angiogenic factor-producing cells. *vegfa* was highly expressed in the ingrown LECs at 1 dpt (Fig.

6a,b and Supplementary Fig. 3f,g), whose expression level was approximately three-fold of the control muLECs (Fig. 6c). Application of SU5416, an inhibitor of the Vegfa signaling, was ineffective to the meningeal lymphatic ingrowth after injury, but led to devoid of neoangiogenesis (Fig. 6d–g and Supplementary Fig. 6). Because Vegfa is also produced by other cell types in the injured area (Fig. 6b, arrowhead), we explore whether the ingrown LEC-produced Vegfa effectively promote the neoangiogenesis. Cellular mosaic animals were generated by early embryonic transplantations to deplete Vegfa in individual meningeal LECs. Controlled by the *Tg(prox1a^{BAC}:KalTA4; UAS:TagRFP; fli1:GFP)* donor embryos injected with a control morpholino (*conMO*), donor cells from the same transgenic background injected with a morpholino against *vegfa* (*vegfaMO*) were transplanted into the *Tg(prox1a^{BAC}:KalTA4; UAS:TagRFP; kdrl:DenNTR)* acceptor embryos. Among all the ingrown lymphatic vessels that originated from the *vegfaMO*-donor cells, only 34.7% of them act as "growing tracks" for nascent blood vessels at 4 dpt, in contrast to 70.3% of those originating from the *conMO*-donor cells (Fig. 6h–k). These data suggest the ingrown meningeal LECs as Vegfa-producing cells that promote the neoangiogenesis.

The ingrown lymphatic vessels undergo apoptosis and clearance after cerebrovascular regeneration is complete

Taken together the data above, meningeal lymphatics rapidly grow into brain parenchyma in response to cerebrovascular damage. On one hand they drain interstitial fluid to resolve brain oedema, on the other hand they act as "growing tracks" to guide the growth of nascent blood vessels and produce Vegfa to promote the neoangiogenesis. However, this ingrown lymphatics-mediated cerebrovascular regeneration mechanism resulted in the presence of lymphatic vessels in the brain parenchyma, inconsistent with its physiologically lymphatic-free status. Therefore, we explored the fate of the ingrown lymphatic vessels after the completion of cerebrovascular regeneration. Time courses using the *lyve1b* or *prox1a* promoter-driven transgenes provided evidences that the ingrown lymphatic vessels gradually disappeared from 5 dpt to 7 dpt (Fig. 7a and Supplementary Fig. 2). Apoptotic signals, detectable in some ingrown LECs from 4 dpt onward (Supplementary Fig. 7), became strong and evident at 6 dpt, but were rarely detectable in the BECs (Fig. 7b–d). These data indicate apoptosis and clearance of the ingrown lymphatic vessels after the completion of cerebrovascular regeneration, so that the brain parenchyma recover the lymphatic-free status.

The ingrown lymphatics-mediated cerebrovascular regeneration is conserved in the zebrafish photochemical thrombosis model

To answer the question whether the ingrowth of meningeal lymphatics occurs in other cerebrovascular injury models, we established another zebrafish model using

photochemical thrombosis, closely mimicking human cerebral thrombosis. The photochemical techniques have been reported to efficiently induce photothrombotic ischemia and damage to local blood vessels in the mouse and rat brain as well as in the zebrafish DA[25-28]. Titrations showed that cold light illumination for 600 seconds after injection of Rose bengal induced thrombosis and damage to blood vessels in the illuminated area of zebrafish brain (Supplementary Fig. 8 and Supplementary Video 6). In contrast to the control injected with Rhodamine (Fig. 8b), meningeal lymphatics invaded the injured area (Fig. 8c, dotted circle) by 2 days post illumination (dpi). Nascent blood vessels (Fig. 8c, arrowheads) grew along the ingrown lymphatics (Fig. 8c, arrow) and cerebrovascular regeneration fulfilled by 4 dpi. At 6 dpi and 7 dpi, the ingrown lymphatic vessels were cleared from the injured area and cerebrovascular regeneration accomplished (Fig. 8c). These results indicate that the meningeal lymphatics-mediated brain vascular regeneration mechanism is conserved in the photochemical thrombosis model.

Discussion

In summary, brain vascular injury induces rapid ingrowth of meningeal lymphatics into the injured brain parenchyma, which is dependent on the locally activated Vegfc. These ingrown lymphatics on one hand become lumenized to drain interstitial fluid from the injured parenchyma to resolve cerebral oedema. On the other hand, they serve as a migratory scaffold to guide the growth of nascent blood vessels and

produce Vegfa to promote the neoangiogenesis (Fig. 7e). Meningeal LECs in zebrafish were nonlumenized and previously called muLECs, BLECs, or FGP cells[10-12]. It is reasonable to refer them as meningeal lymphatics in this study, because they can grow into the injured brain parenchyma and form authentic, lumenized lymphatic vessels. Lumenization is not a prerequisite to be acting as "growing tracks", because growth of nascent blood vessels along nonlumenized lymphatics at 1 dpt and along lumenized lymphatic vessels after 2 dpt have both been observed. Formation of the ingrown lymphatic lumen may be fulfilled through fusion of large vacuoles, which have been reported to be abundant in the muLECs[10,12]. Details and mechanisms of lymphatic lumenization need further comprehensive investigations.

Although the ingrown meningeal lymphatics-mediated brain vascular regeneration mechanism is conserved in the NTR-Mtz and photochemical thrombosis models, we should not conclude that the transient lymphatic vessel is a general response to different types of brain vascular injuries. In a zebrafish cerebrovascular rupture model induced using a focused multi-photon laser, the repair of the rupture is mediated by macrophages through the generation of mechanical traction forces[29], but not mediated by the meningeal lymphatics. Two possible reasons might account for this mechanistic difference. First, both the NTR-Mtz and photochemical thrombosis models induce BEC apoptosis in a certain brain area, whereas laser irradiation model induces blood vessel ruptures. These different types of injuries to blood vessels, "apoptosis" vs "rupture", may explain, at least partially explain, why different vascular repair/regeneration mechanisms are involved. Second, the NTR-Mtz and

photochemical models induce severe brain oedema inside the closed skull, which may be a critical issue to stimulate meningeal lymphatic ingrowth to resolve oedema. The laser irradiation model only damages one blood vessel, which does not cause obvious brain oedema. So, lymphatic vessels are not required to resolve oedema after laser irradiation.

Temporary invasion of meningeal lymphatics prompts a reassessment of the absence of lymphatic vessel in the brain parenchyma, warranting a better understanding of pathological involvements of meningeal lymphatics. "Growing tracks" for nascent blood vessels also expand our knowledge of lymphatic functions. This study in zebrafish provides explanations why VEGFC and VEGFR3 are up-regulated in the rat photothrombotic stroke model[30], and why arteriovenous-malformation human patients express lymphatic-associated genes in the brain[31]. Development of efficacious angiogenic therapies for ischemic stroke is dependent on a thorough understanding of brain vascular regeneration. This study should be informative for the development of translatable post-ischemic therapies, in particular through the application of lymphangiogenic drugs.

Methods

Methods and references, are available in the online version of this paper.

References

1. Krupinski, J., Kaluza, J., Kumar, P., Wang, M. & Kumar, S. Prognostic value of blood vessel density in ischaemic stroke. *Lancet* **342,** 742 (1993).

2. Liu, S. & Levine, S. R. The Continued Promise of Neuroprotection for Acute Stroke Treatment. *J. Exp. Stroke Transl. Med.* **1,** 1–8 (2008).

3. Shen, F. *et al.* Adeno-associated viral vector-mediated hypoxia-regulated VEGF gene transfer promotes angiogenesis following focal cerebral ischemia in mice. *Gene Ther.* **15,** 30–39 (2008).

4. Thored, P. *et al.* Long-term neuroblast migration along blood vessels in an area with transient angiogenesis and increased vascularization after stroke. *Stroke* **38,** 3032–3039 (2007).

5. Greenberg, D.A. & Jin, K. Vascular endothelial growth factors (VEGFs) and stroke. *Cell Mol. Life Sci.* **70**, 1753-1761 (2013).

6. Su, E.J. *et al.* Activation of PDGF-CC by tissue plasminogen activator impairs blood-brain barrier integrity during ischemic stroke. *Nat. Med.* **14**, 731-737 (2008).

7. Heissig, B., Hattori, K., Friedrich, M., Rafii, S. & Werb, Z. Angiogenesis: vascular remodeling of the extracellular matrix involves metalloproteinases. *Curr. Opin. Hematol.* **10,** 136–141 (2003).

8. Aspelund, A. *et al.* A dural lymphatic vascular system that drains brain interstitial fluid and macromolecules. *J. Exp. Med.* **212**, 991-999 (2015).

9. Louveau, A. *et al.* Structural and functional features of central nervous system lymphatic vessels. *Nature* **523**, 337-341 (2015).

10. Bower, N.I. *et al.* Mural lymphatic endothelial cells regulate meningeal angiogenesis in the zebrafish. *Nat. Neurosci.* **20**, 774-783 (2017).

11. Venero Galanternik, M. *et al.* A novel perivascular cell population in the zebrafish brain. *eLife* **6**, e24369 (2017).

12. van Lessen, M. *et al.* Intracellular uptake of macromolecules by brain lymphatic endothelial cells during zebrafish embryonic development. *eLife* **6,** e25932 (2017).

13. Siekmann, A. F. & Lawson, N. D. Notch signalling limits angiogenic cell behaviour in developing zebrafish arteries. *Nature* **445,** 781–784 (2007).

14. Yaniv, K. *et al.* Live imaging of lymphatic development in the zebrafish. *Nat. Med.* **12**, 711-716 (2006).

15. Küchler, A.M. *et al.* Development of the zebrafish lymphatic system requires VEGFC signaling. *Current Biology* **16**, 1244-1248 (2006).

16. Jopling, C. *et al.* Zebrafish heart regeneration occurs by cardiomyocyte dedifferentiation and proliferation. *Nature* **464**, 606-609 (2010).

17. Kikuchi, K. *et al.* Primary contribution to zebrafish heart regeneration by gata4(+) cardiomyocytes. *Nature* **464**, 601-605 (2010).

18. Zhang, R. *et al.* In vivo cardiac reprogramming contributes to zebrafish heart

regeneration. *Nature* **498**, 497-501 (2013).

19. He, J., Lu, H., Zou, Q. & Luo, L. Regeneration of liver after extreme hepatocyte loss occurs mainly via biliary transdifferentiation in zebrafish. *Gastroenterology* **146,** 789–800 (2014).

20. Flores, M.V., Hall, C.J., Crosier, K.E. & Crosier, P.S. Visualization of embryonic lymphangiogenesis advances the use of the zebrafish model for research in cancer and lymphatic pathologies. *Dev. Dyn.* **239**, 2128-2135 (2010).

21. van Impel, A. *et al.* Divergence of zebrafish and mouse lymphatic cell fate specification pathways. *Development* **141**, 1228-1238 (2014).

22. Hogan, B.M. *et al.* Ccbe1 is required for embryonic lymphangiogenesis and venous sprouting. *Nat. Genet.* **41**, 396-398 (2009).

23. Le Guen, L. *et al.* Ccbe1 regulates Vegfc-mediated induction of Vegfr3 signaling during embryonic lymphangiogenesis. *Development* **141**, 1239-1249 (2014).

24. Roukens, M.G. *et al.* Functional Dissection of the CCBE1 Protein: A Crucial Requirement for the Collagen Repeat Domain. *Circ. Res.* **116**, 1660-1669 (2015).

25. Maxwell, K.A. & Dyck, R.H. Induction of reproducible focal ischemic lesions in neonatal mice by photothrombosis. *Dev. Neurosci.* **27**, 121-126 (2005).

26. Lee, J.K. *et al.* Photochemically induced cerebral ischemia in a mouse model. *Surg. Neurol.* **67**, 620-625 (2007).

27. Kuroiwa, T. *et al.* Development of a rat model of photothrombotic ischemia and infarction within the caudoputamen. *Stroke* **40**, 248-253 (2009).

28. Lee, I.J. *et al.* Zebrafish model of photochemical thrombosis for translational research and thrombolytic screening in vivo. *J. Biophotonics.* **10**, 494-502 (2017).

29. Liu, C. *et al.* Macrophages Mediate the Repair of Brain Vascular Rupture through Direct Physical Adhesion and Mechanical Traction. *Immunity* **44**, 1162-1176 (2016).

30. Gu, W., Brannstrom, T., Jiang, W., Bergh, A. & Wester, P. Vascular endothelial growth factor-A and -C protein up-regulation and early angiogenesis in a rat photothrombotic ring stroke model with spontaneous reperfusion. *Acta. Neuropathol.* **102**, 216-226 (2001).

31. Shoemaker, L.D. *et al.* Human brain arteriovenous malformations express lymphatic-associated genes. *Ann. Clin. Transl. Neurol.* **1**, 982-995 (2014).

Acknowledgements

We thank Brant M. Weinstein, Arndt F. Siekmann, Markus Affolter, Elke Ober, Benjamin M. Hogan, Philip S. Crosier, and Naoki Mochizuki for fish lines, antibodies and plasmids. This work was supported by the National Key Basic Research Program of China (2015CB942800), National Natural Science Foundation of China (91539201,

31330051, 31730060, 91739304, 31571508, 31571510), and the 111 Program (B14037).

Author Contributions

L.L., D.Y., and J.C. designed the experimental strategy, analysed data, and wrote the manuscript. J.H. performed the combination of FISH and antibody staining. Q.Y. carried out the CLEM. Y.Z. and T.Z. help analyse data. J.C. performed all the other experiments in the study.

Competing interests

The authors declare no competing financial interests.

Additional information

Supplementary information is available in the online version of this paper.

Figure legends

Fig. 1 | Lymphatic vessels appear in the brain parenchyma after cerebrovascular injury. **a**, **b**, Zebrafish NTR-Mtz brain vascular injury model. In contrast to the control (**a**, n=40/40), brain vasculature of the *Tg(kdrl:DenNTR)* larvae were specifically injured after Mtz treatment (**b**, 0 dpt, n=39/39). Time courses are shown. Arrowheads indicate the remaining relatively large vessels. Arrows indicate the emerging nascent blood vessels. **c**–**e**, In contrast to the absence of lymphangiogenesis in the control (**c**, n=24/24), growth of the *lyve1b*+ lymphatics was rapid and active at 1 dpt after Mtz treatment, but apparently slowed at 2 dpt (**d**, n=20/24). The quantifications show the total length of *kdrl*+ and *lyve1b*+ vessels in the brain at 0-2 dpt (**e**, n=10). **f**, In frontier sections, the *lyve1b*+ lymphatics were predominantly localized in the meninges at the brain surface in the control (#1, n=6/6), whereas became abundant in the brain parenchyma at 1 dpt after Mtz treatment (#1', n=6/6). Scale bar, 50 μm. Mean ± s.e.m., ***P<0.001, Student's t-test.

Fig. 2 | Meningeal lymphatics rapidly grow into the injured parenchyma in response to cerebrovascular damage. **a**, **b**, Time-lapse imaging showed the growth of meningeal lymphatics into the injured area (**a**, n=10/10). Images at the early phases after Mtz treatment showed that the initiation of ingrowth and branching of meningeal lymphatics (**b**, n=10/10). The elapsed time is indicated in hours:minutes after 0 dpt. **c**–**g**, Cre/loxP-based lineage tracing showed that the ingrown vessels are of the

lymphatic origin. Transgenic lines, time points of Mtz and 4-OHT administrations are shown in (**c**). Negatively controlled by Mtz plus ethanol (**d**, n=12/12) and positively controlled by DMSO plus 4-OHT (**e**, n=19/21), the ingrown vessels were double positive for anti-DsRed and anti-GFP antibodies if Mtz plus 4-OHT were applied (**f**, n=21/24). The statistics show the ratios of the *lyve1b:DsRed*-labelled vessels positive for GFP (**g**, n=10). Scale bars, 50 μm. Mean ± s.e.m., ***P<0.001, Student's t-test.

Fig. 3 | Ingrowth of meningeal lymphatics is dependent on the locally activated Vegfc. **a–c**, Expression of *vegfc* at 1 dpt (**a**, n=30/34). Approximately 68% and 22% of the FISH-*vegfc* signals are distributed in the BECs and *nkx2.2*+ neurons (**a**, arrowhead), respectively (**b**, n=10). RT-qPCRs using dissected brain tissues show the relative expression levels of *vegfc* in the brain at 1-5 dpt (**c**, n=5). **d–f**, In contrast to the absence of *vegfr3* in the control (**d**, n=18/20), *vegfr3* is exclusively expressed in the *fli1+kdrl-* LECs at 1 dpt (**e**, n=17/22). Higher magnification images of the framed areas are displayed. The statistics show the ratios of vessels positive for *vegfr3* (**f**, n=15). **g–j**, After Mtz treatment, meningeal lymphatic ingrowth (*fli1+kdrl-*) and neoangiogenesis (*kdrl+*) did not occur in the *ccbe1* mutant (**h**, n=23/27) in contrast to the wild-type (**g**, n=36/40). The quantifications show the total lengths of the ingrown lymphatics at 1 dpt (**i**, n=6) and nascent blood vessels (BVs) at 3 dpt (**j**, n=6). **k–m**, In contrast to the wild-type (**k**, n=16/16), the *ccbe1* mutant at 3 dpt exhibited severe cerebral oedema (**l**, n=17/17) indicated as significantly enlarged inter-optic distance (red lines), which is confirmed by statistical analysis (**m**, n=9). All scale bars are 50

μm. Mean ± s.e.m., ***P<0.001, *P<0.05, Student's t-test.

Fig. 4 | The ingrown meningeal lymphatics undergo lumenization to drain brain interstitial fluid. a, Illustrations of DA and ICV injection points. **b**, **c**, Rhodamine filled in the blood vessels (arrowheads), but remained absent in the ingrown lymphatics (arrows) after DA injection (**b**, n=8/10). Drainage of Rhodamine was rapidly observed in the ingrown meningeal lymphatic vessels (mLVs) after ICV injection (**c**, n=15/16). **d**–**i**, Endocytosis, but not lumen flow, of Alexa647-IgG was observed in the meningeal LECs (mLECs) after ICV injection into the control larvae (**d**, n=15/15), or into the Mtz-treated larvae at 1 dpt (**f**, n=12/13). Thirty minutes later, the endocytosed dye maintained and accumulated in the mLECs (**e**, n=14/14; **g**, n=11/12). If the Alexa647-IgG was injected at 2 dpt after Mtz treatment, the dye filled in the lumen of lymphatic vessels immediately after injection (**h**, n=17/20). Thirty minutes later, the dye was drained out from the lumen, but the endocytosed dye remained in the mLECs (**i**, n=16/20). Note that the lumen of lymphatics was clearly visible under confocal microscope at 2 dpt (**h**, arrows), but not in the control (**d**) or at 1 dpt (**f**). Scale bar, 50 μm.

Fig. 5 | The ingrown meningeal lymphatics act as "growing tracks" for nascent blood vessels through direct physical adhesion. a, Time-lapse imaging showed that the nascent blood vessel (*kdrl*+, arrows) grew along the preformed lymphatic vessel

(*fli1+kdrl-*, arrowheads). Bright field indicated the two vessel structures. The elapsed time is indicated in hours:minutes. Scale bar, 10 μm. **b**, **c**, Ablation of the ingrown lymphatic vessel (**c**, n=20/20 vessels in 10 larvae, 2 vessels per larvae), but not the neighbouring parenchyma (**b**, n=20/20 sites in 10 larvae, 2 sites per larvae), led to the growth arrest and regression of the adhering nascent blood vessel (arrowheads). Arrows indicate the laser irradiation sites. The elapsed time is indicated in hours:minutes. Scale bar, 20 μm. **d**, **e**, In contrast to its absence in the control brain (**d**, n=21/22), Claudin5b was enriched at the interface between the ingrown lymphatic (*prox1a+*) and nascent blood vessels (*kdrl+*) after Mtz treatment (**e**, n=18/21). **f–h**, Correlative light and electron microscopy (CLEM) at 2 dpt. (**f**) The FIB-SEM target area inside confocal images is indicated with frame. Scale bar, 10 μm. (**g**) 3D-reconstructions of FIB-SEM planes identify the ingrown meningeal lymphatic vessel (mLV) and nascent blood vessel (BV) as two adhering vessel structures (n=3/3). The framed area in (**f**) is shown in (**g**). (**h**) Single FIB-SEM image plane indicates the lumens of mLV and BV (n=3/3). Light green and light red mark the cross sections of lymphatic vessel and blood vessel, respectively. Their junctional line represents tight junctions (TJ, arrow). Scale bar, 1 μm.

Fig. 6 | The ingrown meningeal LECs produce Vegfa to promote the neoangiogensis. **a–c**, In contrast to the control (**a**, n=21/22), *vegfa* expression at 1 dpt was observed in the ingrown meningeal LECs and other cell types (arrowhead) (**b**, n=17/20). RT-qPCRs using *lyve1b+* cells sorted from the brain confirmed the elevated

expression level of *vegfa* in the ingrown LECs than in the physiological muLECs (**c**, n=5). Scale bar, 50 μm. **d–g**, In contrast to the normal lymphatic ingrowth and neoangiogenesis in the control (**d**, n=22/23), SU5416 blocked the neoangiogenesis, but left the meningeal lymphatic ingrowth unaffected (**e**, n=19/22). Total lengths of the meningeal lymphatics at 1 dpt (**f**, n=8) and the ratios of lymphatic vessel with nascent blood vessel growing along at 3 dpt (**g**, n=8) were exhibited. Scale bar, 50 μm. Mean ± s.e.m., ***$P < 0.001$, NS, not significant, Student's *t*-test. **h–k**, Generation of Vegfa mosaic animals by cell transplantations. If a *conMO* was injected into donor embryos, the majority of *prox1a*+GFP+ lymphatic vessels that originated from the donor cells were "growing tracks" of nascent blood vessels in the acceptor larvae (**h**, n=109/155 vessels, 70.3%). The ratio of *prox1a*+GFP- lymphatic vessels (originate from acceptors themselves) acting as "tracks" is similar (**i**, n=320/463 vessels, 69.1%). In contrast, among all the ingrown meningeal lymphatics originating from the *vegfaMO*-donor cells (*prox1a*+GFP+), the majority of them failed to be "growing tracks" for nascent blood vessels (**j**, n=126/193 vessels, 65.3%), whereas the majority of *prox1a*+GFP- vessels (originate from acceptors themselves) still acted as "tracks" (**k**, n=361/527 vessels, 68.5%). Scale bar, 20 μm.

Fig. 7 | The ingrown lymphatic vessels undergo apoptosis after the completion of cerebrovascular regeneration. a, The ingrown lymphatic vessels disappeared from 6 dpt to 7 dpt (n=23/26). Arrowhead and arrows indicate the adhering lymphatic and blood vessels, respectively. Note the disappearance of the lymphatic vessel at 7 dpt

(dotted arrowhead). Scale bar, 20 μm. **b–d**, In contrast to the control (**b**, n=33/35), TUNEL signals were detected in approximately 70% of the meningeal lymphatic vessels (*fli1*+*kdrl*-) (**c**, n=30/33), but in less than 5% of the blood vessels (*kdrl*+) (**d**, n=8). Scale bar, 20 μm. Mean ± s.e.m., ***P<0.001, Student's t-test. **e**, Illustrations of brain vascular regeneration promoted and guided by the temporarily ingrown meningeal lymphatics. BV, blood vessel.

Fig. 8 | The temporarily ingrown lymphatics-mediated cerebrovascular regeneration mechanism is conserved in the photochemical brain thrombosis model. a, Technical procedures of the photochemical thrombosis in the zebrafish brain. **b**, Injection of Rhodamine followed by illumination was ineffective to local brain blood vessels (n=10/10). **c**, One day post injection of Rosa bengal and a 600-second illumination (1 dpi), local cerebrovascular damage was evident in the illuminated area (dotted circle). By 2 dpi, meningeal lymphatics (arrow) grew into the injured area. Nascent blood vessels grew along the ingrown lymphatics, and the neoangiogenesis fulfilled by 4 dpi. At 6 dpi and 7 dpi, the ingrown lymphatics become cleared from the injured area (n=15/20). Arrowheads indicate the leading edge of growing blood vessels. Scale bar, 50 μm.

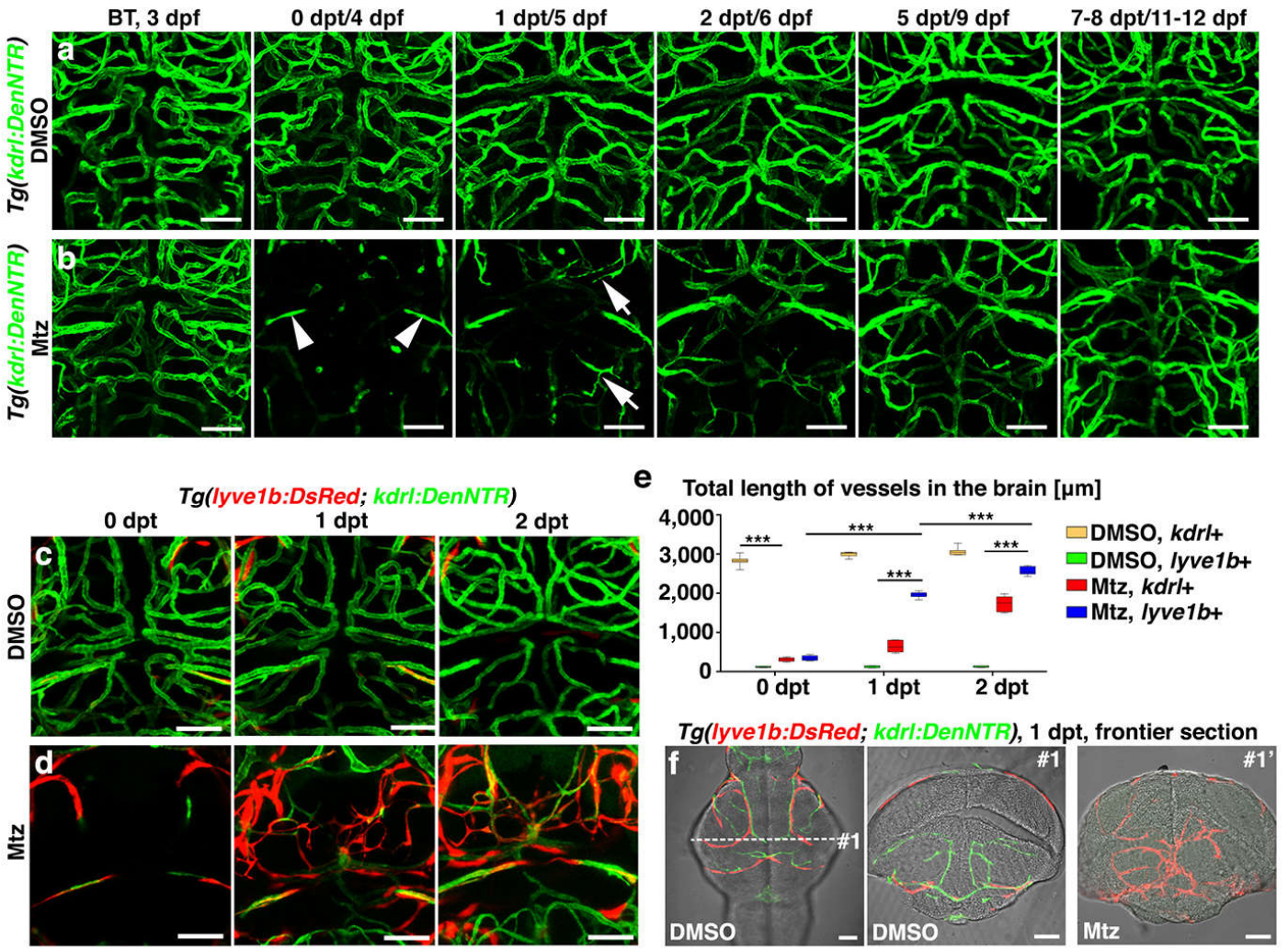
BT, 3 dpf
0 dpt/4 dpf
1 dpt/5 dpf
2 dpt/6 dpf
5 dpt/9 dpf
7-8 dpt/11-12 dpf
a
b
Tg(kdrl:DenNTR)
DMSO
Mtz
Tg(lyve1b:DsRed; kdrl:DenNTR)
0 dpt
1 dpt
2 dpt
c
d
e
Total length of vessels in the brain [µm]
4,000
3,000
2,000
1,000
0
***
DMSO, kdrl+
DMSO, lyve1b+
Mtz, kdrl+
Mtz, lyve1b+
Tg(lyve1b:DsRed; kdrl:DenNTR), 1 dpt, frontier section
f
#1
#1'
DMSO
Mtz

Luo_Figure 1

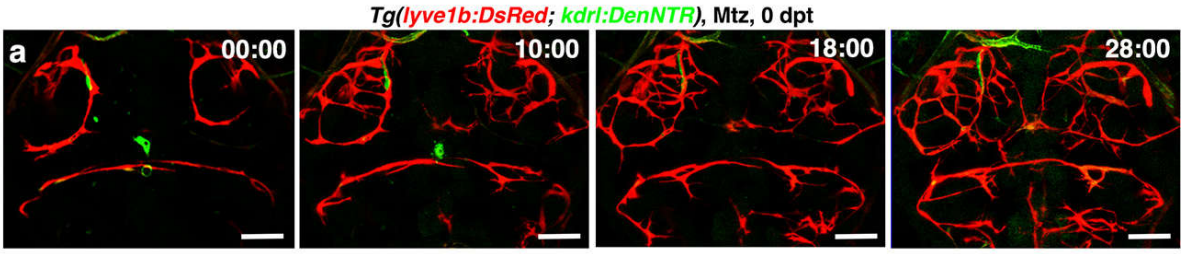
Tg(lyve1b:DsRed; kdrl:DenNTR), Mtz, 0 dpt
a
00:00
10:00
18:00
28:00

Tg(lyve1b:DsRed; kdrl:DenNTR), Mtz, 0 dpt
b
3D-reconstruction
00:00
02:50
06:50

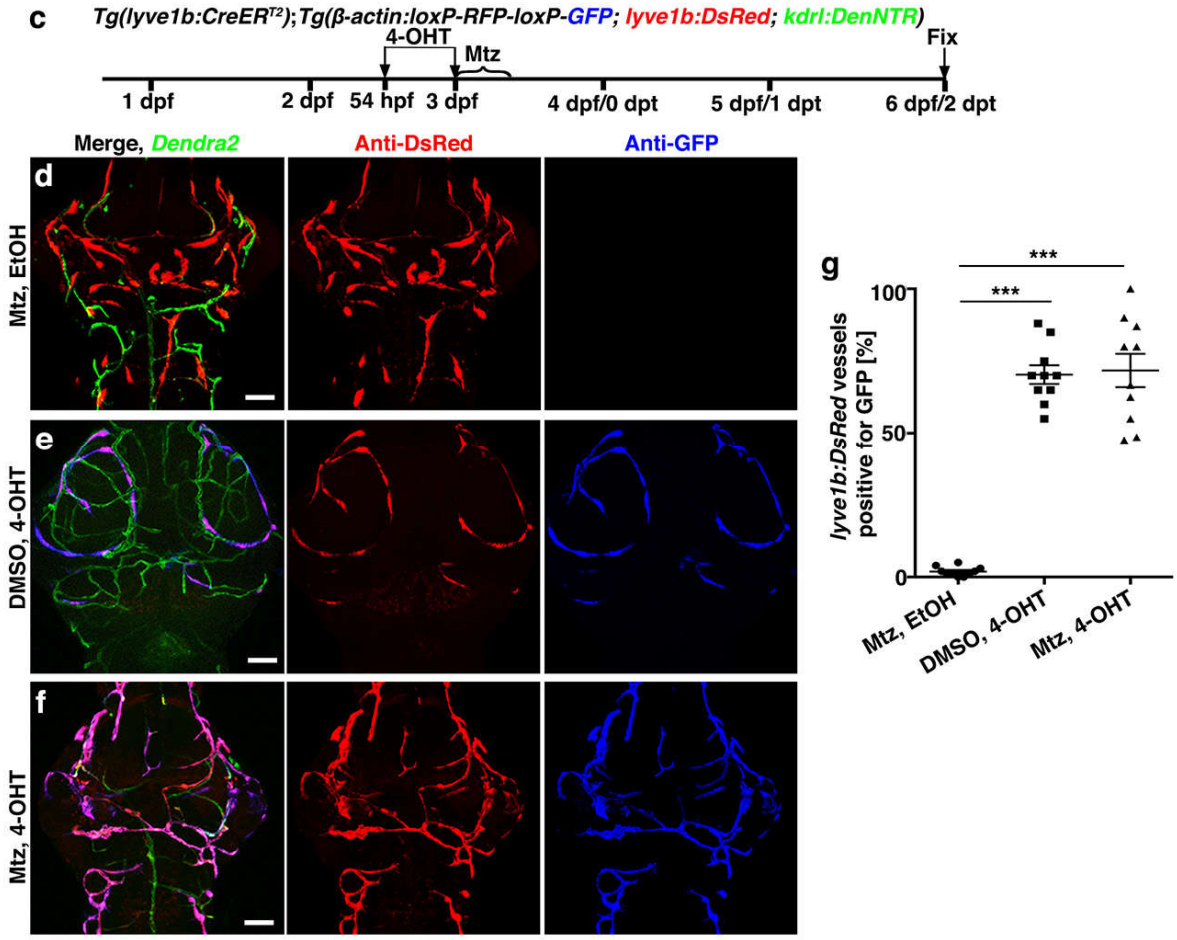
c
Tg(lyve1b:CreER^{T2});Tg(β-actin:loxP-RFP-loxP-GFP; lyve1b:DsRed; kdrl:DenNTR)
4-OHT
Mtz
Fix
1 dpf
2 dpf
54 hpf
3 dpf
4 dpf/0 dpt
5 dpf/1 dpt
6 dpf/2 dpt
Merge, Dendra2
Anti-DsRed
Anti-GFP
d
e
f
Mtz, EtOH
DMSO, 4-OHT
Mtz, 4-OHT
g
lyve1b:DsRed vessels positive for GFP [%]
100
50
0
***
***
Mtz, EtOH
DMSO, 4-OHT
Mtz, 4-OHT

Luo_Figure 2

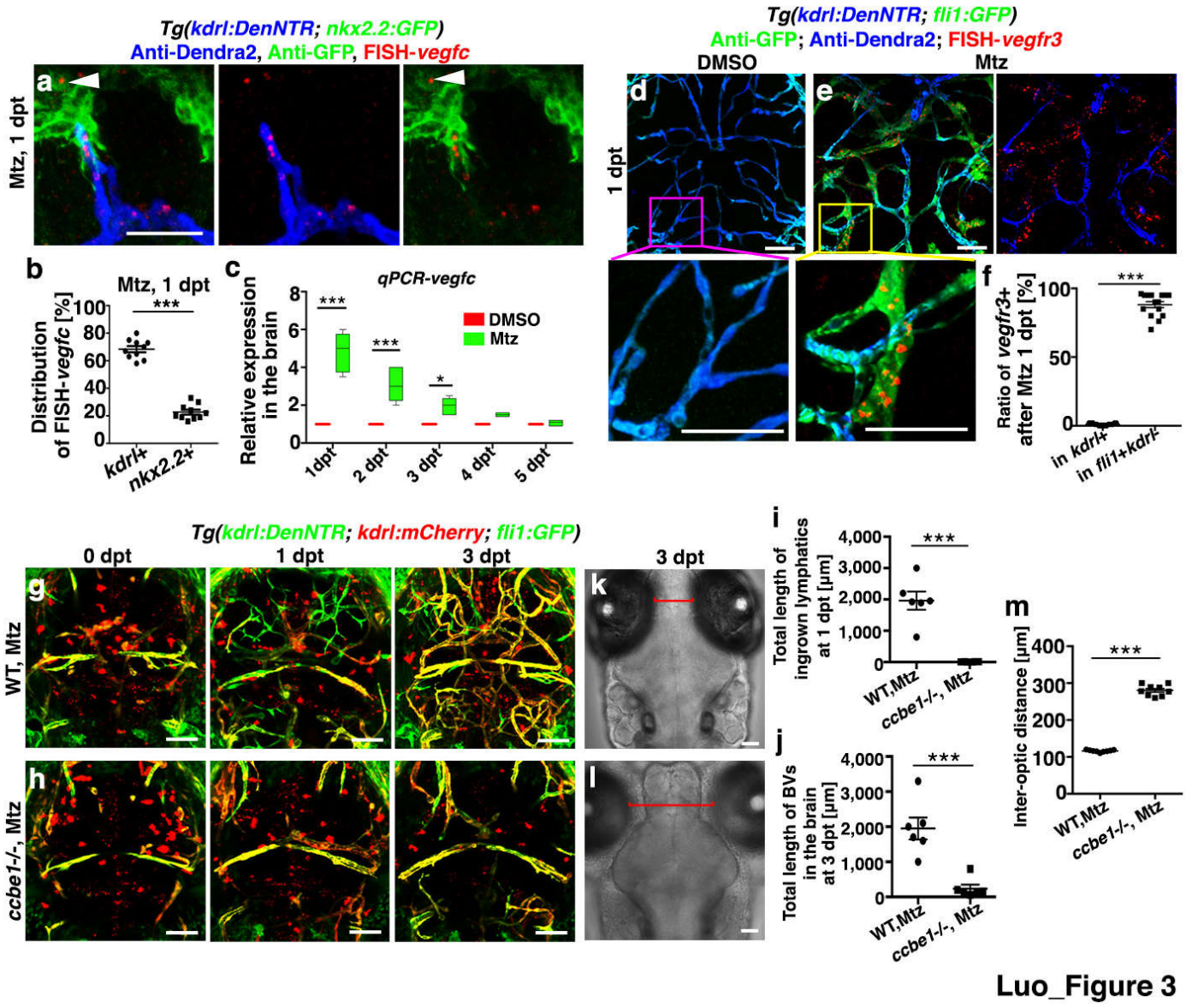
Tg(kdrl:DenNTR; nkx2.2:GFP)
Anti-Dendra2, Anti-GFP, FISH-vegfc
Mtz, 1 dpt
a
b
Mtz, 1 dpt
Distribution of FISH-vegfc [%]
***
kdrl+
nkx2.2+
c
qPCR-vegfc
Relative expression in the brain
DMSO
Mtz
***
***
*
1dpt
2 dpt
3 dpt
4 dpt
5 dpt
Tg(kdrl:DenNTR; fli1:GFP)
Anti-GFP; Anti-Dendra2; FISH-vegfr3
DMSO
Mtz
1 dpt
d
e
f
Ratio of vegfr3+ after Mtz 1 dpt [%]
***
in kdrl+
in fli1+kdrl-
Tg(kdrl:DenNTR; kdrl:mCherry; fli1:GFP)
0 dpt
1 dpt
3 dpt
3 dpt
WT, Mtz
ccbe1-/-, Mtz
g
h
k
l
i
Total length of ingrown lymphatics at 1 dpt [µm]
***
WT,Mtz
ccbe1-/-, Mtz
j
Total length of BVs in the brain at 3 dpt [µm]
***
WT,Mtz
ccbe1-/-, Mtz
m
Inter-optic distance [µm]
***
WT,Mtz
ccbe1-/-, Mtz

Luo_Figure 3

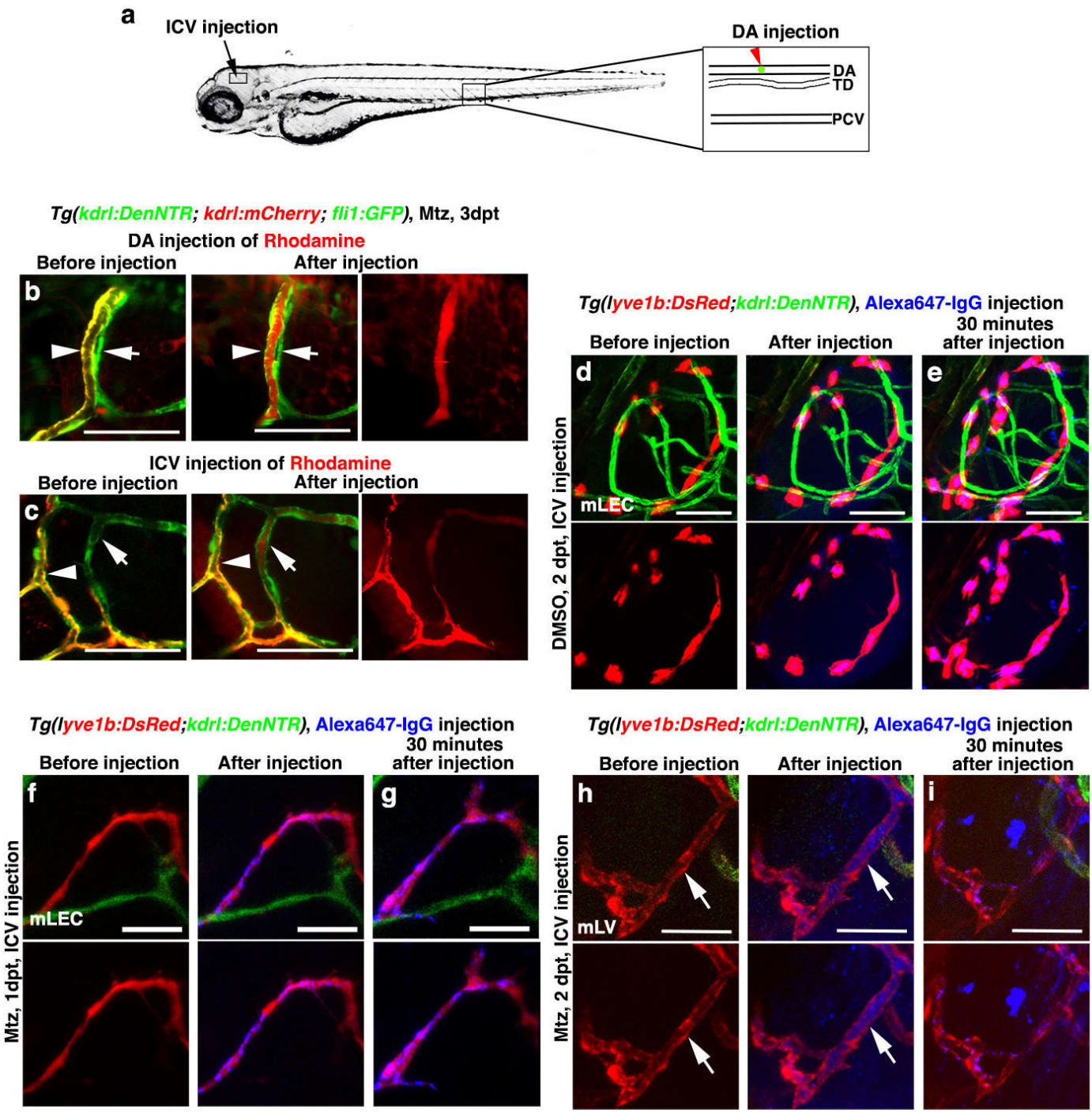
a
ICV injection
DA injection
DA
TD
PCV
Tg(kdrl:DenNTR; kdrl:mCherry; fli1:GFP), Mtz, 3dpt
DA injection of Rhodamine
Before injection
After injection
b
ICV injection of Rhodamine
Before injection
After injection
c
Tg(lyve1b:DsRed;kdrl:DenNTR), Alexa647-IgG injection
Before injection
After injection
30 minutes after injection
d
e
mLEC
DMSO, 2 dpt, ICV injection
Tg(lyve1b:DsRed;kdrl:DenNTR), Alexa647-IgG injection
Before injection
After injection
30 minutes after injection
f
g
mLEC
Mtz, 1dpt, ICV injection
Tg(lyve1b:DsRed;kdrl:DenNTR), Alexa647-IgG injection
Before injection
After injection
30 minutes after injection
h
i
mLV
Mtz, 2 dpt, ICV injection

Luo_Figure 4

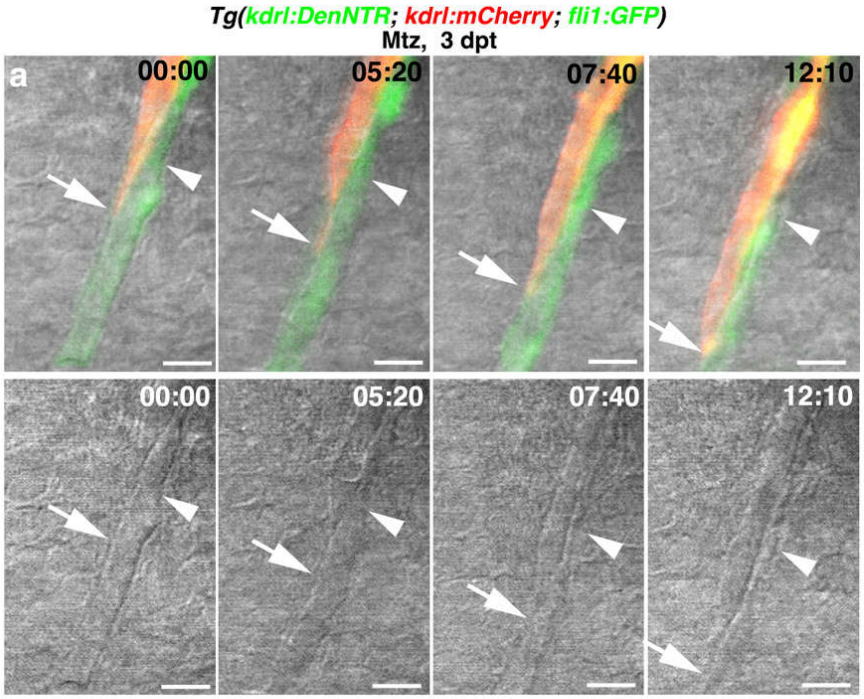
Tg(kdrl:DenNTR; kdrl:mCherry; fli1:GFP)
Mtz, 3 dpt
a
00:00
05:20
07:40
12:10
00:00
05:20
07:40
12:10

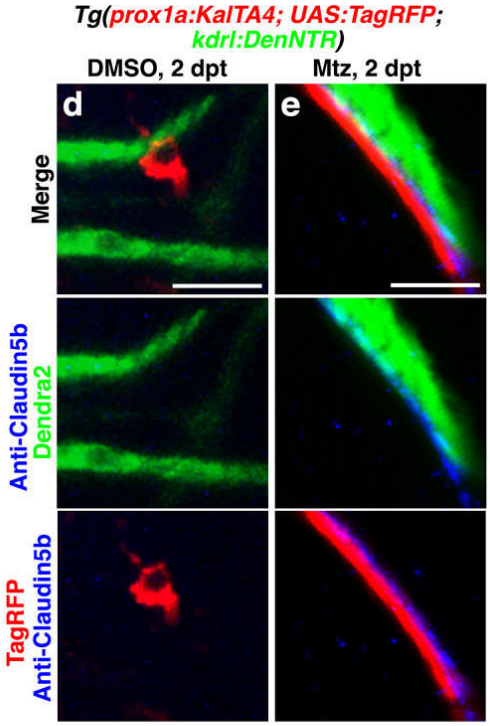
Tg(prox1a:KalTA4; UAS:TagRFP; kdrl:DenNTR)
DMSO, 2 dpt
Mtz, 2 dpt
d
e
Merge
Anti-Claudin5b
Dendra2
TagRFP
Anti-Claudin5b

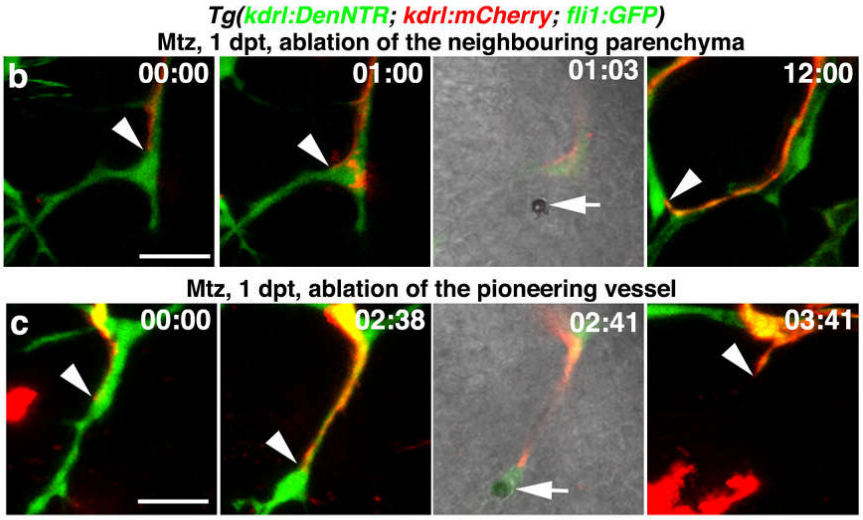
Tg(kdrl:DenNTR; kdrl:mCherry; fli1:GFP)
Mtz, 1 dpt, ablation of the neighbouring parenchyma
b
00:00
01:00
01:03
12:00
Mtz, 1 dpt, ablation of the pioneering vessel
c
00:00
02:38
02:41
03:41

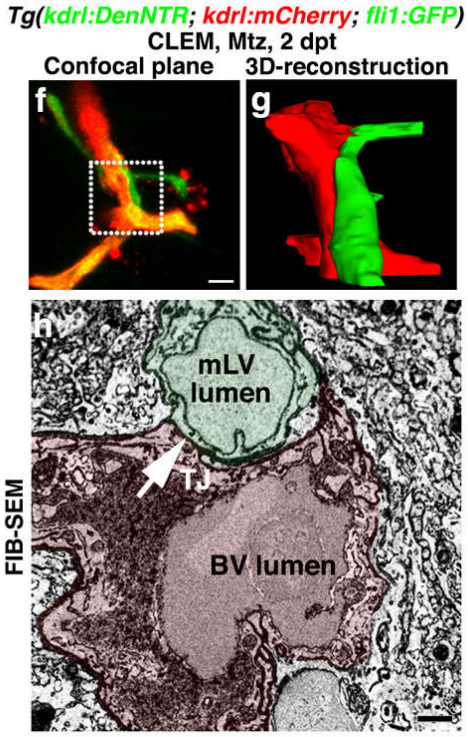
Tg(kdrl:DenNTR; kdrl:mCherry; fli1:GFP)
CLEM, Mtz, 2 dpt
Confocal plane
3D-reconstruction
f
g
h
FIB-SEM
mLV lumen
TJ
BV lumen

Luo_Figure 5

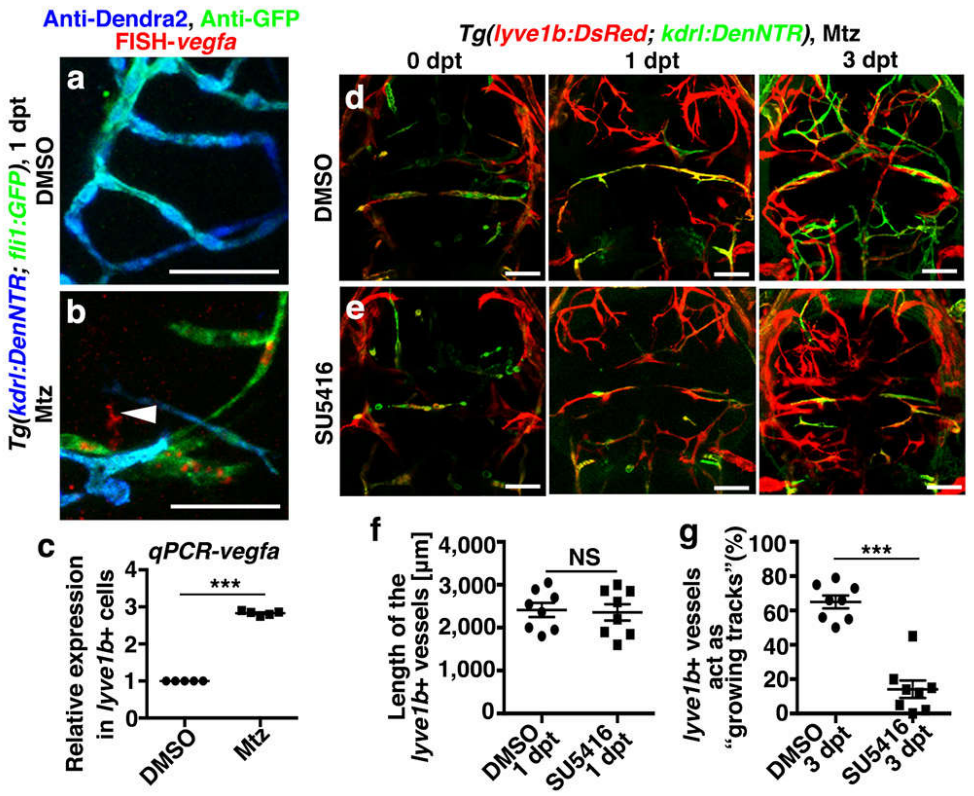
Anti-Dendra2, Anti-GFP
FISH-vegfa
Tg(kdrl:DenNTR; fli1:GFP), 1 dpt
DMSO
Mtz
a
b
Tg(lyve1b:DsRed; kdrl:DenNTR), Mtz
0 dpt
1 dpt
3 dpt
DMSO
SU5416
d
e
c
qPCR-vegfa
Relative expression in lyve1b+ cells
***
DMSO
Mtz
f
Length of the lyve1b+ vessels [µm]
NS
DMSO 1 dpt
SU5416 1 dpt
g
lyve1b+ vessels act as "growing tracks"(%)
***
DMSO 3 dpt
SU5416 3 dpt

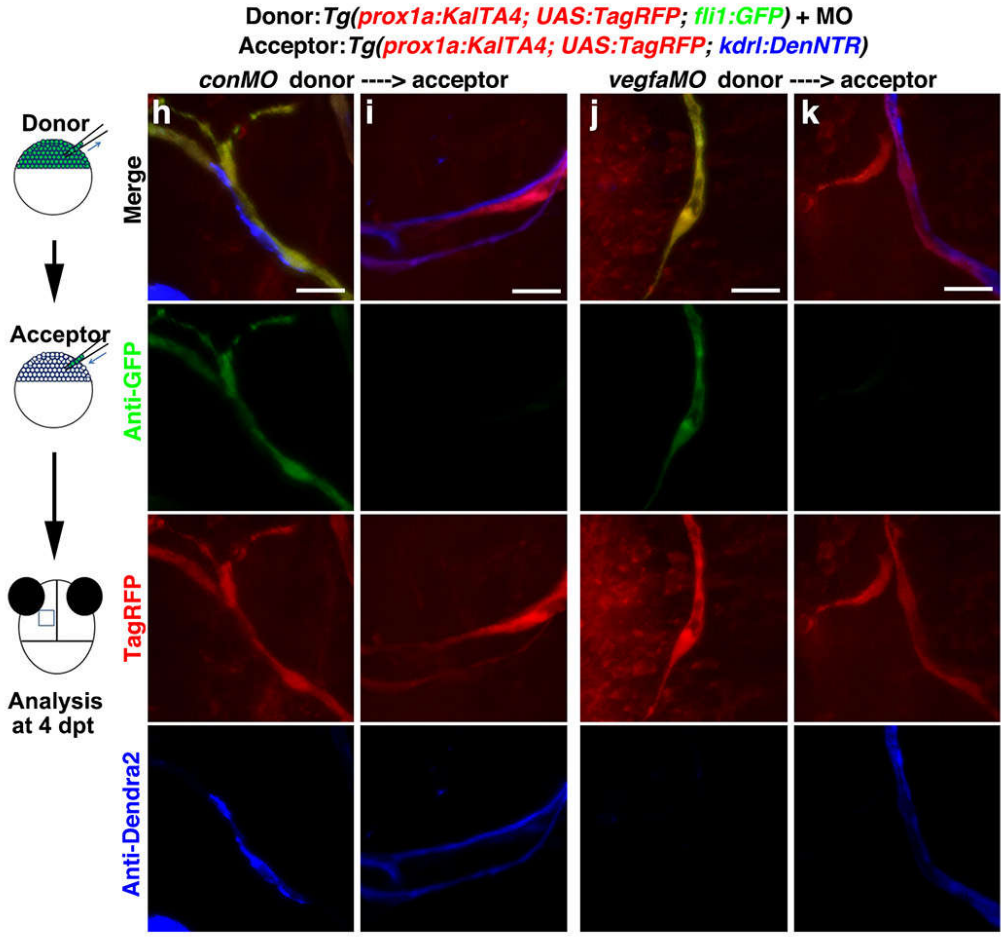
Donor: Tg(prox1a:KalTA4; UAS:TagRFP; fli1:GFP) + MO
Acceptor: Tg(prox1a:KalTA4; UAS:TagRFP; kdrl:DenNTR)
conMO donor ----> acceptor
vegfaMO donor ----> acceptor
Donor
Acceptor
Analysis at 4 dpt
Merge
Anti-GFP
TagRFP
Anti-Dendra2
h
i
j
k

Luo_Figure 6

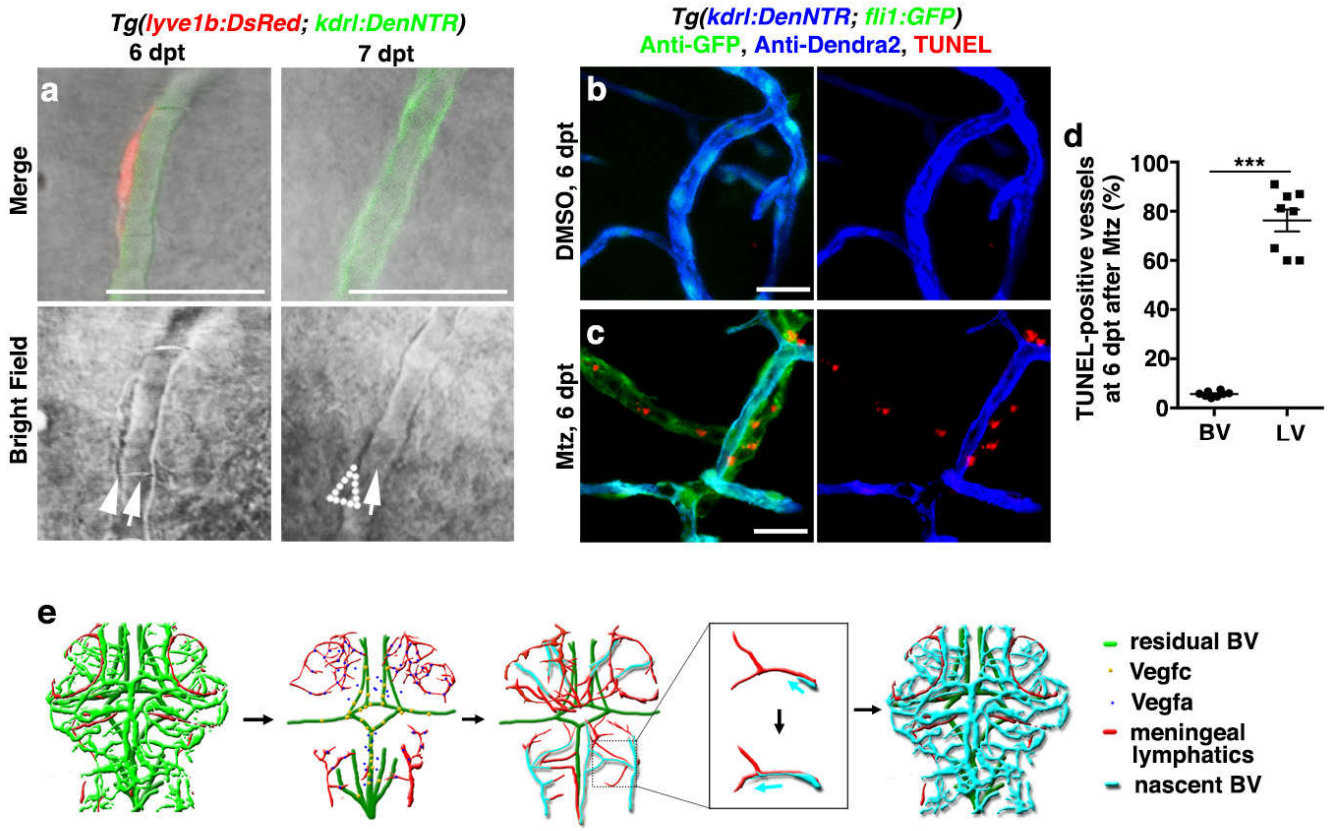
Tg(lyve1b:DsRed; kdrl:DenNTR)
6 dpt
7 dpt
a
Merge
Bright Field
Tg(kdrl:DenNTR; fli1:GFP)
Anti-GFP, Anti-Dendra2, TUNEL
b
c
DMSO, 6 dpt
Mtz, 6 dpt
d
TUNEL-positive vessels at 6 dpt after Mtz (%)
100
80
60
40
20
0
***
BV
LV
e
residual BV
Vegfc
Vegfa
meningeal lymphatics
nascent BV

Luo_Figure 7

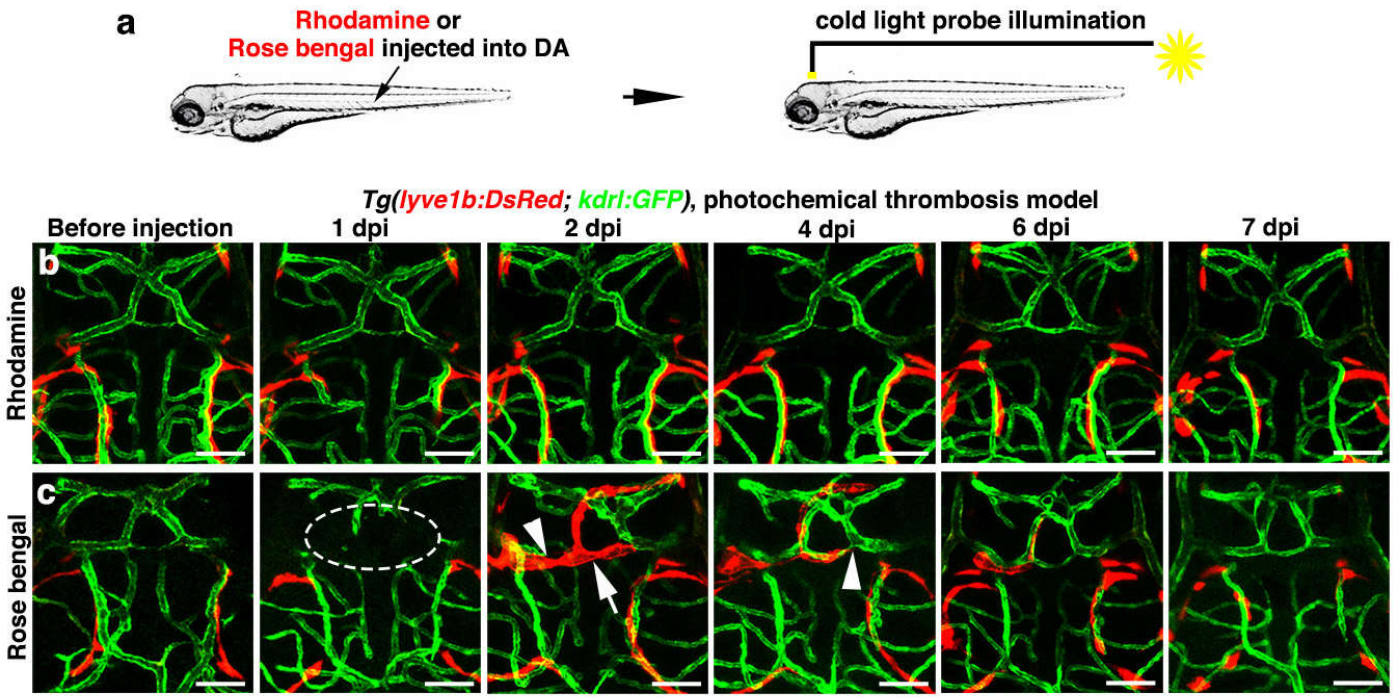
a
Rhodamine or
Rose bengal injected into DA
cold light probe illumination
Tg(lyve1b:DsRed; kdrl:GFP), photochemical thrombosis model
Before injection
1 dpi
2 dpi
4 dpi
6 dpi
7 dpi
b
Rhodamine
c
Rose bengal

Luo_Figure 8